^{15}N NMR Relaxation Studies of the FK506 Binding Protein: Backbone Dynamics of the Uncomplexed Receptor

Jya-Wei Cheng, Christopher A. Lepre, Stephen P. Chambers, John R. Fulghum, John A. Thomson, and Jonathan M. Moore*

Vertex Pharmaceuticals Incorporated, 40 Allston Street, Cambridge, Massachusetts 02139-4211

Received April 12, 1993; Revised Manuscript Received June 7, 1993

ABSTRACT: Backbone dynamics of the major tacrolimus (FK506) binding protein (FKBP-12, 107 amino acids) have been studied using ^{15}N relaxation data derived from proton-detected two-dimensional ^{1}H–^{15}N NMR spectroscopy. ^{15}N spin–lattice relaxation rate constants (R_1), spin–spin relaxation rate constants (R_2), and heteronuclear NOEs were determined for over 85% of the backbone amide ^{15}N nuclei. A model free formalism [Lipari, G., & Szabo, A. (1982) *J. Am. Chem. Soc. 104,* 4546–4559; Lipari, G., & Szabo, A. (1982) *J. Am. Chem. Soc. 104,* 4559–4570] was used to derive values for the generalized order parameter (S^2), the effective correlation time for internal motions (τ_e), and the chemical exchange line width (R_{ex}) for each N–H bond vector. The final optimized overall correlation time (τ_m) was 9.2 ns. The average order parameter (S^2) describing the amplitude of motions on the picosecond time scale was found to be 0.88 ± 0.06. Motions on the picosecond time scale are restricted at the N and C termini, consistent with previous NMR structural studies indicating well-defined β-strands in these regions. With the exception of the flap region from residues 82 to 87, no regions appear to be significantly disordered on the picosecond time scale. Residues in several regions of the protein exhibit high R_{ex} terms, indicating possible motions on the millisecond to microsecond time scale due to chemical exchange and/or conformational averaging effects. Possible effects of tacrolimus (FK506) binding on FKBP-12 dynamics are discussed in the context of previously determined solution structures for FKBP-12 in the uncomplexed [Michnick et al. (1991) *Science 252,* 836–839; Moore et al. (1991) *Nature 351,* 248–250] and complexed [Meadows et al. (1993) *Biochemistry 32,* 754–765] states.

Rational drug design is based on the premise that novel, potent therapeutics may be synthesized on the basis of a detailed knowledge of the three-dimensional structures of target proteins and protein–inhibitor complexes. Current implementations of the structure-based approach involve the iterative use of physical methods such as X-ray crystallography and solution NMR[1] in assessing the relationship between the three-dimensional structures and biological activities of potential therapeutic agents (Appelt et al., 1991; Baldwin et al., 1989; Kuntz, 1992; Navia & Murcko, 1992). X-ray crystallographic methods, in general, are capable of providing rapid structural feedback to computational and synthetic chemists. NMR methods, while currently not as rapid as X-ray crystallography, can also provide structural information in the form of solution structures for receptor–ligand complexes or, via isotope editing techniques, the bound conformations of drugs or drug candidates [e.g., Lepre et al. (1992), Fesik et al. (1991), Petros et al. (1992a,b), and Weber et al. (1991)]. Both methods of structure determination, however, provide the chemist with only static models of the receptor or receptor–ligand complex.

Since it is well established that the motions of protein molecules on several distinct time scales may be directly related to their biological function, it follows that a more useful model of a potential drug target requires both structural and dynamic aspects; one should not only determine the coordinates of the target protein but also assess the rates and magnitudes with which those coordinates change over time.

NMR spectroscopy is uniquely suited to characterize the internal motions of proteins on time scales ranging from picoseconds to seconds or longer. Recently, the development of proton-detected heteronuclear NMR methods, along with the use of ^{15}N isotope labeling strategies, has resulted in a number of reports characterizing both the internal and overall motions of small proteins (Kay et al., 1989; Clore et al., 1990a; Palmer et al., 1991; Barbato et al., 1992; Berglund et al., 1992; Kördel et al., 1992; Peng & Wagner, 1992a; Powers et al., 1992; Redfield et al., 1992; Schneider et al., 1992; Skelton et al., 1992; Stone et al., 1992, 1993). Interpretation of experimental relaxation data and subsequent characterization of molecular motions on the picosecond time scale have been pursued either by using the model free formalism (Lipari & Szabo, 1982a,b) or, more rigorously, via direct spectral density mapping (Peng & Wagner, 1992b).

FKBP-12 (M_r = 11 800) belongs to a group of immunomodulatory proteins termed immunophilins (Schreiber, 1991; Rosen & Schreiber, 1992; Sigal & Dumont, 1992). The most widely studied immunophilins include FKBP-12 and cyclophilin (M_r = 17 000). These two proteins, which share no amino acid sequence or structural similarities, both catalyze the interconversion of the cis–trans rotamers of peptidyl–prolyl amide bonds. These proteins are also the major intracellular receptors for the potent immunosuppressants tacrolimus (FK506) and cyclosporin A, which bind to FKBP-12 and cyclophilin, respectively. Both immunosuppressants appear to act by blocking signal transduction pathways leading

* Author to whom correspondence should be addressed.

[1] Abbreviations: CPMG, Carr–Purcell–Meiboom–Gill; CSA, chemical shift anisotropy; DQ, double quantum; FKBP-12, FK506 binding protein (M_r ~11 800); GARP, globally optimized alternating-phase rectangular pulses; HSQC-NOESY, heteronuclear single-quantum coherence nuclear Overhauser enhancement spectroscopy; INEPT, insensitive nuclei enhancement by polarization transfer; IPTG, isopropyl β-D-thiogalactopyranoside; NMR, nuclear magnetic resonance; NOE, nuclear Overhauser enhancement; R_1, longitudinal relaxation rate constant; R_2, transverse relaxation rate constant; T_1, longitudinal relaxation time; T_2, transverse relaxation time; TPPI, time-proportional phase incrementation.

0006-2960/93/0432-9000$04.00/0

to T-cell activation. It has been demonstrated (Bierer et al., 1990) that inhibition of the peptidyl–prolyl cis–trans isomerase activity of these proteins is not sufficient for immunosuppression. Rather, both protein–drug complexes bind to and inhibit a common target, the calcium- and calmodulin-dependent protein phosphatase, calcineurin (Liu et al., 1991, 1992). Both immunosuppressants have also been shown to block translocation of a cytoplasmic component of the transcription factor NF-AT to the cell nucleus, preventing the formation of mature NF-AT and the consequent transcription of cytokine genes necessary for the immune response (Flanagan et al., 1991). The relationship between calcineurin inhibition and nuclear translocation of immature NF-AT remains unclear.

Recently, much effort has been directed toward determination of the three-dimensional structures of immunophilins and immunophilin–drug complexes using both X-ray crystallography (Kallen et al., 1991; Kallen & Walkinshaw, 1992; Ke et al., 1991; Pflügl et al., 1993; Van Duyne et al., 1991a,b, 1993) and multidimensional NMR methods (Fesik et al., 1991, 1992; Hsu & Armitage, 1992; Lepre et al., 1992; Meadows et al., 1993; Michnick et al., 1991; Moore et al., 1991; Weber et al., 1991; Wüthrich et al., 1991; Petros et al., 1992a,b; Spitzfaden et al., 1992; Thériault et al., 1993).

To better understand the influence of FK506 binding on the internal dynamics of FKBP-12 and to complement the high-resolution, yet static models of protein structure provided by the above studies, we have used inverse-detected two-dimensional ^{1}H–^{15}N NMR experiments to examine the backbone dynamics of uncomplexed FKBP-12. Amide ^{15}N relaxation data were analyzed using the model free formalism of Lipari and Szabo (1982a,b) and interpreted in terms of the generalized order parameter (S^2), the effective correlation time for fast internal motions (τ_e), and the chemical exchange line width (R_{ex}). The addition of information concerning protein backbone dynamics to the static models obtained from X-ray crystallography and NMR spectroscopy should prove useful in the development of new immunosuppressive drugs via a structure-based approach.

MATERIALS AND METHODS

Sample Preparation. High-level expression of human recombinant FKBP-12 in *Escherichia coli* has been achieved by the construction of vectors containing the complete sequence for the gene subcloned behind a phage T7 RNA polymerase promoter vector (Studier et al., 1990). Protein production is then achieved by the addition of isopropyl β-D-thiogalactopyranoside (IPTG) which induces a chromosomal copy of T7 RNA polymerase (behind the *lac* UV promoter) in the host JM109/DE3, which in turn starts transcription of the protein gene (Studier & Moffat, 1986). With this promoter system, 20–30% of the total cellular protein is human recombinant FKBP-12 after induction.

Uniform ^{15}N and ^{13}C isotopically labeled human recombinant FKBP-12 was produced in *E. coli* grown in M9 minimal media (Maniatis et al., 1986) with [^{15}N, 99%]ammonium chloride (1 g/L) and sodium [2-^{13}C, 99%]acetate (3 g/L) as the sole nitrogen and carbon sources, respectively (Venters et al., 1991). Growth was initiated by inoculating M9 salts/glucose media with a single colony from a freshly streaked plate. The seed colony was grown at 37 °C until mid-log phase and then diluted 1:50 into the main culture. In the M9 minimal/acetate media JM109/DE3 grows to its mid-log phase with a doubling time of 4 h, at which point it is induced with 1 mM IPTG. The culture was harvested once growth had stopped, and the typical yield of cell paste was 20 g from a 10-L fermentor (Biostat ED, B. Braun). This sample was purified as described previously (Moore et al., 1991). Approximately 200 mg of purified protein was obtained from 20 g of cell paste. The final NMR sample contained 8.6 mM human recombinant FKBP-12 in 50 mM potassium phosphate buffer (90% H_2O, 10% D_2O) at pH 7.0. ^{15}N incorporation was >95% and ^{13}C incorporation was 60–70% as determined by examination of resolved resonances in decoupled (^{15}N and ^{13}C) and nondecoupled 1D NMR spectra.

NMR Spectroscopy. All NMR experiments were recorded at 500.13 MHz (^{1}H) and 50.68 MHz (^{15}N) on a Bruker AMX-500 spectrometer equipped with a three-channel interface and triple-resonance probe. All measurements were carried out at 303 K. The sensitivity-enhanced ^{1}H-detected pulse sequences used to measure ^{15}N T_1 and T_2 relaxation times and {^{1}H}–^{15}N NOEs were based on those described previously by Kördel et al. (1992). Subspectra collected from sensitivity-enhanced T_1 or T_2 experiments were combined on an IRIS 4D/35 workstation using software written in-house. Subspectra in the NOE experiments (with or without proton saturation) were processed separately to yield two independent measurements of the heteronuclear NOE.

T_1 and T_2 experiments were collected with a spectral width of 3521 Hz in the F_2 domain and 2534 Hz in the F_1 domain with the ^{1}H carrier frequency set to the center of the amide proton region. NOE experiments were acquired with a spectral width of 8064.5 Hz in the F_2 domain and with the ^{1}H carrier frequency set to the water signal. All spectra were acquired in the phase-sensitive mode using time-proportional phase incrementation (TPPI) (Marion & Wüthrich, 1983) for quadrature detection in F_1. The water signal in all experiments was suppressed by low-power presaturation and by using high-power spin-lock purge pulses (Messerle et al., 1989) with a field strength of 29.4 kHz. Time domain data were recorded with 2048 complex points in t_2 and with 300 real points in the indirectly detected dimension; 16 transients per t_1 increment were acquired for both T_1 and T_2 experiments, while 32 transients per increment were collected for the heteronuclear NOE experiment. ^{15}N and ^{13}C decoupling during t_2 was carried out using GARP decoupling (Shaka & Keeler, 1987), whereas decoupling during the t_1 period was achieved using a hard ^{1}H 180° pulse. ^{15}N and ^{13}C carrier frequencies were set to 50.6844 and 125.773 MHz, respectively.

For T_1 and T_2 experiments, a relaxation delay of 1.8 s was used between acquisitions. For NOE experiments, a relaxation delay of 4.8 s was used to ensure the maximal development of NOEs before acquisition and to allow solvent to relax ($T_1 \approx 4$ s). The time interval between the refocusing pulses in the CPMG (Meiboom & Gill, 1958) period of the T_2 experiments was set to 1.0 ms to effectively spin-lock the heteronuclear spins. High-power ^{15}N pulses of 5-kHz field strength used in the T_2 experiments were generated with an auxiliary amplifier (Model 3205, American Microwave Technology). Eight delays of 33, 108, 184, 270, 346, 562, 1081, and 2054 ms were used during the inversion–recovery period of the T_1 experiments, whereas eight delays of 4, 19, 34, 57, 67, 76, 95, and 115 ms were used during the CPMG period of the T_2 experiments.

T_1, T_2, and NOE spectra were processed on an Iris 4D/35 workstation using the software FELIX (Biosym Technologies, San Diego, CA). Time domain data were multiplied by a cosine squared bell function before Fourier transformation in both frequency dimensions. Final matrices contained 1K × 1K real points after zero-filling and Fourier transformation.

Polynomial baseline corrections were applied in all cases in the F_2 domain after Fourier transformation.

In order to observe those amide protons that undergo slow exchange with solvent, an unlabeled, aqueous FKBP-12 sample was transferred into D_2O buffer over a 2-h period by multiple buffer exchanges in an Amicon ultrafiltration cell, giving a final concentration of 4.4 mM FKBP-12 in 50 mM potassium phosphate, pD 7.4. Slowly exchanging amides were identified primarily from a clean-TOCSY spectrum (70-ms isotropic mixing time) (Griesinger et al., 1988) collected immediately after buffer exchange. Additionally, overlapped amides were identified from the fingerprint region of a double-quantum (DQ) spectrum (Braunschweiler et al., 1983; Rance & Wright, 1986) and an HSQC-NOESY spectrum (Bax et al., 1990; Norwood et al., 1990) acquired later on a uniformly ^{15}N-labeled sample. Due to the long collection times used, we classify as slowly exchanging all amides which are persistent in the above NMR spectra after a period of 12 h.

Determination of ^{15}N Relaxation Parameters. The relaxation rate constants (R_1 and R_2) were determined from nonlinear least squares fits of the experimental peak heights to two- or three-parameter single exponential functions using routines kindly provided by Dr. Arthur G. Palmer, Columbia University. Criteria for choosing between the two- and three-parameter fits were the same as employed by Palmer et al. (1991). Peak heights were measured for all cross-peaks using routines within FELIX (Biosym Technologies, San Diego, CA). Uncertainties in measured peak heights were estimated by comparing values for pairs of resonances arising from the side-chain amides of Gln and Asn residues in the first T_1 and T_2 experiments. Uncertainties estimated in this manner were comparable to those estimated from the RMS baseline noise level and ranged from 1.5% to 3.5% of the total peak height. Uncertainties in the calculated rate constants were determined from the covariance matrix. Heteronuclear NOEs were calculated as the ratios of cross-peak heights recorded with and without proton saturation, and errors were estimated by comparison of NOE values derived from the two independently processed data sets acquired using the sensitivity-enhanced NOE experiment (Kördel et al., 1992).

Model Free Calculations. The spin relaxation of a peptide amide ^{15}N nucleus is dominated by the dipolar interaction between the ^{15}N nucleus and the attached ^1H nucleus, as well as the chemical shift anisotropy (CSA). In the present study, although uniformly labeled [^{13}C,^{15}N]FKBP-12 was used, the dipolar interaction between the nearer of the two ^{13}C nuclei and the backbone amide ^{15}N is less than 2% of that from the directly bonded amide proton, due to the low gyromagnetic ratio of ^{13}C and the relatively long carbon–nitrogen bond length (1.33 Å). Thus, the relaxation contributions from carbon–nitrogen mechanisms are less than experimental error compared to those from nitrogen–proton. The ^{15}N longitudinal (R_1) and transverse (R_2) relaxation rate constants and the heteronuclear NOEs are given by the combinations of the five spectral density functions listed in eqs 1–3

$$R_1 = \left(\frac{d^2}{4}\right)[J(\omega_H - \omega_N) + 3J(\omega_N) + 6J(\omega_H + \omega_N)] + c^2J(\omega_N) \quad (1)$$

$$R_2 = \left(\frac{d^2}{8}\right)[4J(0) + J(\omega_H - \omega_N) + 3J(\omega_N) + 6J(\omega_H) + 6J(\omega_H + \omega_N)] + \left(\frac{c^2}{6}\right)[4J(0) + 3J(\omega_N)] + \pi R_{ex} \quad (2)$$

$$\mathrm{NOE} = 1 + \left(\frac{d^2}{4R_1}\right)\left(\frac{\gamma_H}{\gamma_N}\right)[6J(\omega_H + \omega_N) - J(\omega_H - \omega_N)] \quad (3)$$

in which

$$d = \frac{\mu_0}{4\pi}\gamma_H\gamma_N\frac{h}{2\pi}\langle r_{NH}^{-3}\rangle \quad (4)$$

$$c = \frac{\omega_N(\sigma_\parallel - \sigma_\perp)}{\sqrt{3}} \quad (5)$$

where μ_0 is the permeability of free space, h is Planck's constant, γ_H and γ_N are the gyromagnetic ratios of ^1H and ^{15}N, r_{NH} is the nitrogen–proton bond length (1.02 Å), and ω_H and ω_N are the Larmor frequencies of ^1H and ^{15}N. The difference between the parallel ($\sigma_\parallel$) and perpendicular ($\sigma_\perp$) components of the chemical shift tensor was set to −160 ppm (Hiyama et al., 1988). The R_{ex} term in eq 2 represents line broadening due to chemical exchange and/or conformational averaging on a time scale slower than the overall rotational correlation time.

Because the number of experimental observables (R_1, R_2, NOE) is not sufficient to explicitly determine the five spectral density values, a simpler model for the spectral density may be invoked. As described in detail elsewhere (Lipari & Szabo, 1982a,b; Clore et al., 1990b), the model free approach characterizes both the rate and amplitude of internal motion for individual N–H bond vectors using two parameters. The effective correlation time (τ_e) depends on the rate of motion for fluctations of the amide bond vector occurring on time scales faster than the overall rotational correlation time (τ_m) of the molecule. The generalized order parameter (S^2) is a dimensionless parameter describing the spatial extent of motion of the N–H bond unit vector. Values for the generalized order parameter may range from $S^2 = 0$, indicating completely isotropic motion, to $S^2 = 1$, describing completely restricted motion. The model free formalism may be applied to describe the motions of either isotropically or anisotropically reorienting proteins in solution.

Since the three principal components of the inertial tensor of FKBP-12 were calculated to be approximately 1.0:0.90:0.97 from both NMR (Moore et al., 1991) and X-ray crystallographic structures (M. M. Yamashita, S. H. Rotstein, M. A. Murcko, K. P. Wilson, J. Boger, J. A. Thomson, M. J. Fitzgibbon, and M. A. Navia, unpublished results), we may treat FKBP-12 as an isotropically tumbling molecule.

The spectral density function from the model free formalism for an isotropically tumbling protein is

$$J(\omega) = (2/5)\left[\frac{S^2\tau_m}{1 + (\omega\tau_m)^2} + \frac{(1 - S^2)\tau}{1 + (\omega\tau)^2}\right] \quad (6)$$

where

$$1/\tau = 1/\tau_m + 1/\tau_e$$

If the time scale of the internal motions is fast ($\tau_e < 10$ ps), the spectral density function of eq 6 can be reduced to

$$J(\omega) = (2/5)\frac{S^2\tau_m}{1 + (\omega\tau_m)^2} \quad (7)$$

The model free parameters were obtained by substitution of either eq 6 or 7 into eqs 1–3, followed by optimization using the experimental measurements of the relaxation rate constants R_1 and R_2 and the heteronuclear NOE enhancement. Optimizations were carried out using software provided by Dr. Arthur G. Palmer, Columbia University, following previously

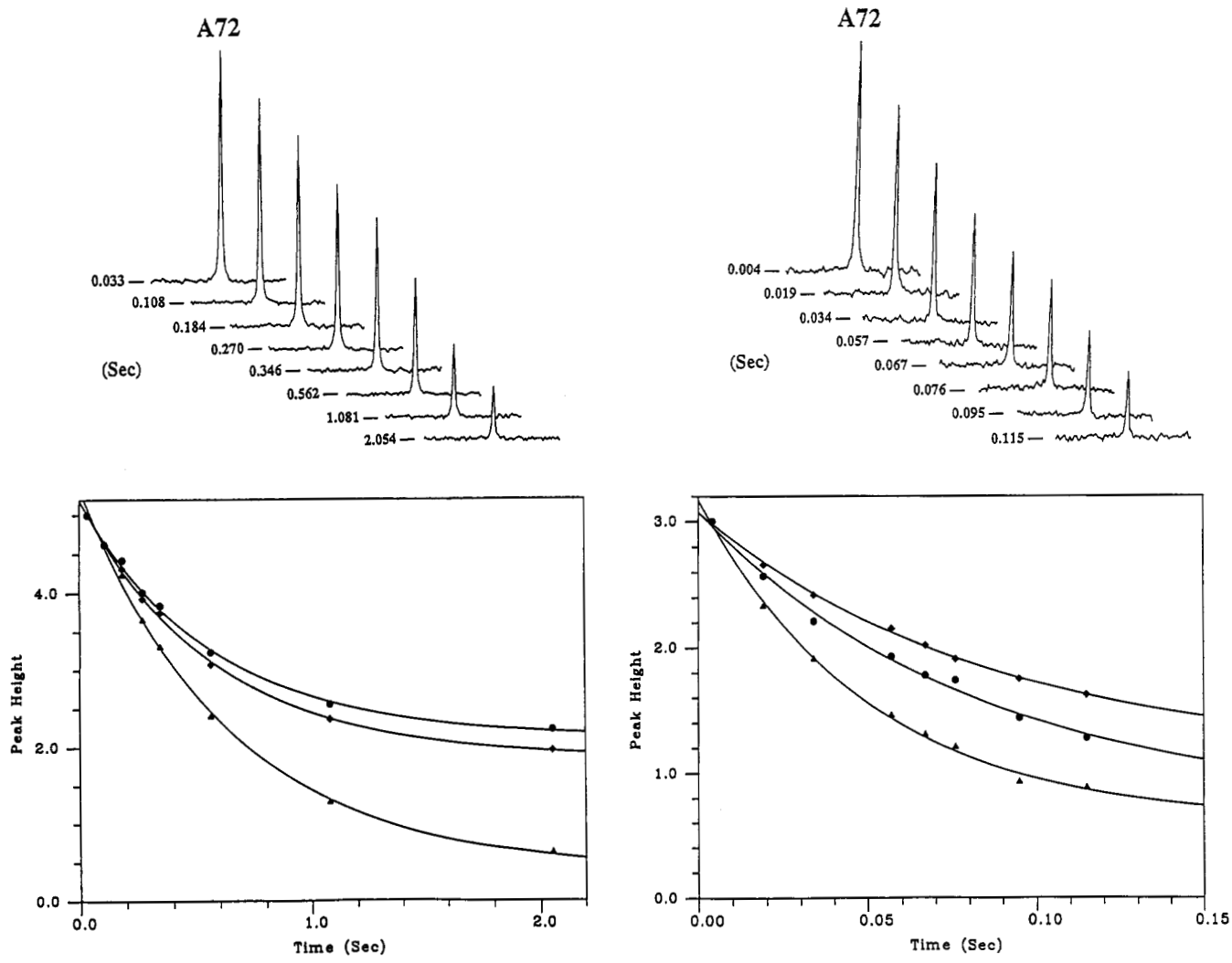

FIGURE 1: Typical decay curves. Shown in panels a and b (top left and top right) are F_2 cross sections of residue A72 taken from the two-dimensional T_1 and T_2 experiments, respectively. (a, bottom left) Fitted decaying curves for the spin–lattice relaxation rate constants (R_1) of residues A72 (●), L74 (◆), and Q65 (▲). (b, bottom right) Fitted decay curves for the spin–spin relaxation rate constants (R_2) of residues A72 (●), M49 (◆), and L50 (▲). For the inversion recovery (T_1) experiments, peaks were phased positive rather than negative for display purposes. Decay curves shown are normalized to the same value for the first data point to facilitate comparison.

published procedures (Palmer et al., 1991; Kördel et al., 1992; Stone et al., 1992).

RESULTS

Figure 1 shows cross sections taken from the two-dimensional spectra of A72 for the T_1 and T_2 experiments, respectively, and illustrates the quality of the experimental data. Complete backbone amide nitrogen and proton assignments for FKBP-12 at pH 5.0 have been reported previously (Rosen et al., 1991) and have been verified using a number of two- and three-dimensional NMR experiments under present sample conditions (Lepre and Moore, unpublished results). Of the 99 backbone amide protons (107 residues minus 7 Pro and N-terminal Gly), 94 can be found in the $\{^1H\}$–^{15}N heteronuclear NOE experiments and 92 are visible in the double INEPT ^1H–^{15}N T_1 and T_2 experiments. Asp79 and Thr85 were excluded from the calculations because of their weak cross-peak intensities in the T_1 and T_2 experiments. Thus, quantitative measurements could be made for approximately 85% of the total backbone amide groups. For Ser38, Arg42, Asp79, and Thr85, cross-peaks could be seen only in the NOE experiments, and qualitative estimates of the dynamics for these residues were made on the basis of NOE measurements.

Determination of ^{15}N Relaxation Rate Constants R_1 and R_2. Several typical fitted monoexponential decay curves showing cross-peak height versus relaxation delay in the T_1 and T_2 experiments are displayed in Figure 1. The standard deviations of the fitted R_1 and R_2 values were less than 10%, with the majority being less than 5%. The mean spin–lattice relaxation rate constant, R_1, was 1.65 ± 0.14 s^{-1}. Only ten residues, V2, K35, F36, K44, K47, K52, G83, G86, H87, and A95, were found to have R_1 values that were smaller than the average by one standard deviation or more. Most of these residues are located in loop regions that appeared ill-defined in previous NMR structural studies (Moore et al., 1991). For reference, Figure 2 shows the X-ray crystal structure (M. M. Yamashita, S. H. Rotstein, M. A. Murcko, K. P. Wilson, J. Boger, J. A. Thomson, M. J. Fitzgibbon, and M. A. Navia, unpublished results) of bovine thymus FKBP-12 with residue numbers.

The fitted transverse relaxation rate constants (R_2) have values ranging from 10.90 to 32.98 s^{-1} in different regions. For 29 residues located in the best defined regions of the NMR and X-ray structures (mostly in the β-sheet region), a mean R_2 value of 11.97 ± 0.58 s^{-1} was derived. These amides are known to be hydrogen-bonded from the observation of slow D_2O exchange and cross-sheet NOEs (Moore et al., 1991;

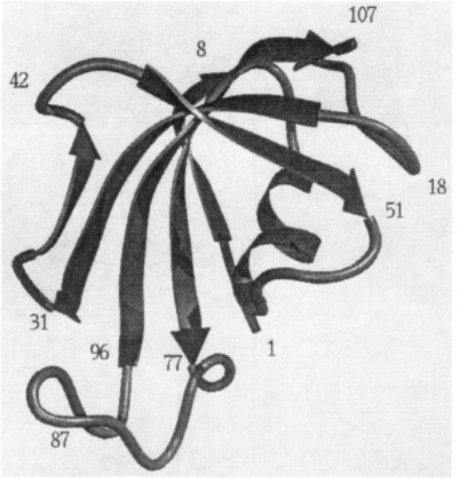

FIGURE 2: Ribbon diagram of bovine FKBP-12 (M. M. Yamashita, S. H. Rotstein, M. A. Murcko, K. P. Wilson, J. Boger, J. A. Thomson, M. J. Fitzgibbon, and M. A. Navia, unpublished results), drawn with the program Quanta (Polygen, Waltham, MA). The bovine and human recombinant proteins are highly homologous, containing only three conservative substitutions at V49M, N94H, and I98V.

Lepre and Moore, unpublished results). The ^{15}N R_1 and R_2 values and their errors are plotted as a function of residue number in Figure 3.

Determination of Heteronuclear NOEs. For most of the residues, including the N and C termini, NOE values were observed to be larger than 0.75, indicating that internal motions on the fast (picosecond) time scale are restricted. As pointed out in other studies (Clore et al., 1990a; Powers et al., 1992), systematic errors in the measurement of heteronuclear NOEs may arise due to chemical exchange between water and amide protons, which can result in a 10–20% increase in the relative magnitude of the experimental NOEs. For several residues, the experimental NOEs are greater than the theoretical maximum of 0.82. For these residues, NOEs were not used in the first optimization, and an average value of 0.82 ± 0.1 was back-calculated from the R_1 and R_2 values. This back-calculated average value was used for all further optimizations. Values determined for the ^{15}N–^1H NOE are also shown in Figure 3.

Initial Estimation of the Overall Rotational Correlation Time. The overall rotational correlation time, τ_m, was estimated using the R_2/R_1 ratios for a set of 29 selected residues mentioned above. These residues were selected because they were located in regions which were well-defined in both the solution and crystal structures. Residues located in regions of regular secondary structure or supersecondary structure are less likely to undergo conformational averaging and/or chemical exchange effects, which would result in shorter measured values of T_2. The procedures followed for optimization of τ_m were similar to those reported in previous relaxation studies (Kay et al., 1989; Clore et al., 1990a; Palmer et al., 1991; Stone et al., 1992, 1993). Using the selected R_2/R_1 values, τ_m was optimized to be 9.5 ± 0.5 ns for 8.6 mM FKBP-12 at 303 K. The value of τ_m obtained in the present study is comparable to those reported for small proteins in previous studies (Kay et al., 1989; Clore et al., 1990a; Barbato et al., 1992; Berglund et al., 1992; Kördel et al., 1992; Peng & Wagner, 1992a; Powers et al., 1992; Redfield et al., 1992; Schneider et al., 1992; Stone et al., 1992, 1993) but appears somewhat long for a protein of 107 amino acids tumbling isotropically. One possibility is that this longer value for τ_m arises due to solution viscosity effects in such a concentrated (8.6 mM) NMR sample.

Analysis of Model Free Parameters. There are several different protocols that can be used to obtain model free parameters based on experimental data. In previous studies (Clore et al., 1990a), the mean and standard deviations of T_1/T_2 values were used as criteria to select the applicable model free formalisms, i.e., eqs 6 and 7, in the optimization process. An extended model free formalism may be warranted if the simulated NOEs based on the optimized S^2 and τ_e values differ from the experimental data (Clore et al., 1990b). Another procedure employs a series of Monte Carlo simulations to select values for the different terms of the model free formalism and then includes those terms with nonzero values in further cycles of optimization (Palmer et al., 1991; Kördel et al., 1992; Stone et al., 1992, 1993). This latter method was adopted in the present study because it allows easier incorporation of both τ_e and R_{ex} terms for a single residue. Detailed procedures for this model free analysis can be found in the recent study by Stone et al. (1993). Briefly, using the initially estimated τ_m of 9.52 ns in the Monte Carlo simulations, if the optimized values of τ_e and/or R_{ex} were nonzero, then τ_e and/or R_{ex} was (were) optimized in the final calculation. Otherwise, τ_e and/or R_{ex} was set to zero. A final calculation was performed by optimizing not only S^2, τ_e, and R_{ex} (if necessary) but also τ_m. The final optimized τ_m was found to be 9.18 ± 0.17 ns, which is close to the original estimate derived from the subset of R_2/R_1 ratios for well-defined residues as described above. The optimized model free parameters S^2, τ_e, and R_{ex} for FKBP-12 are plotted as a function of residue number in Figure 4, and the values are listed in Table I. The reliability of the fits was judged by comparing the R_1, R_2, and NOE values obtained from Monte Carlo simulations with the experimental data. The differences between simulated and experimental results were typically less than 10%.

The average value of the order parameter for FKBP-12 was found to be 0.88, with a range from 0.66 for G86 to 0.95 for V101. For most of the residues, order parameters were larger than 0.85, indicating that rapid motions were largely restricted. On the other hand, a significant number of residues displayed R_{ex} values greater than 2.0 Hz, indicating that chemical or conformational exchange processes occurring on a slower time scale are present within a large portion of the protein molecule. Values of the optimized order parameter S^2 and exchange line width R_{ex} found for backbone amide groups are shown in color in Figure 5. Nonzero values for τ_e are observed for 71 N–H bond vectors in uncomplexed FKBP-12. Most values are in the range 10–50 ps, with the largest values occurring at residue 33 and in a loop region from residues 53 to 56. No residues in FKBP-12 exhibited motions on a time scale of 0.5–4.0 ns; therefore, the extended model free analysis of Clore et al. (1990a,b) was not required.

DISCUSSION

^{15}N Relaxation Measurements. The experimental parameters measured in heteronuclear relaxation studies, namely, R_1, R_2, and the heteronuclear NOE, are dependent on the spectral densities at five characteristic frequencies, $J(0)$, $J(\omega_N)$, $J(\omega_H - \omega_N)$, $J(\omega_H)$, and $J(\omega_H + \omega_N)$, and are sensitive to molecular motions on the picosecond to nanosecond time scales. If the model free formalism is used to approximate the spectral density functions at these frequencies, then experimental measurement of R_1, R_2, and NOE can be used to characterize internal motions in terms of the generalized order parameter, S^2, and a parameter (τ_e) which can be related to the effective correlation time for fast internal motions for each amide bond

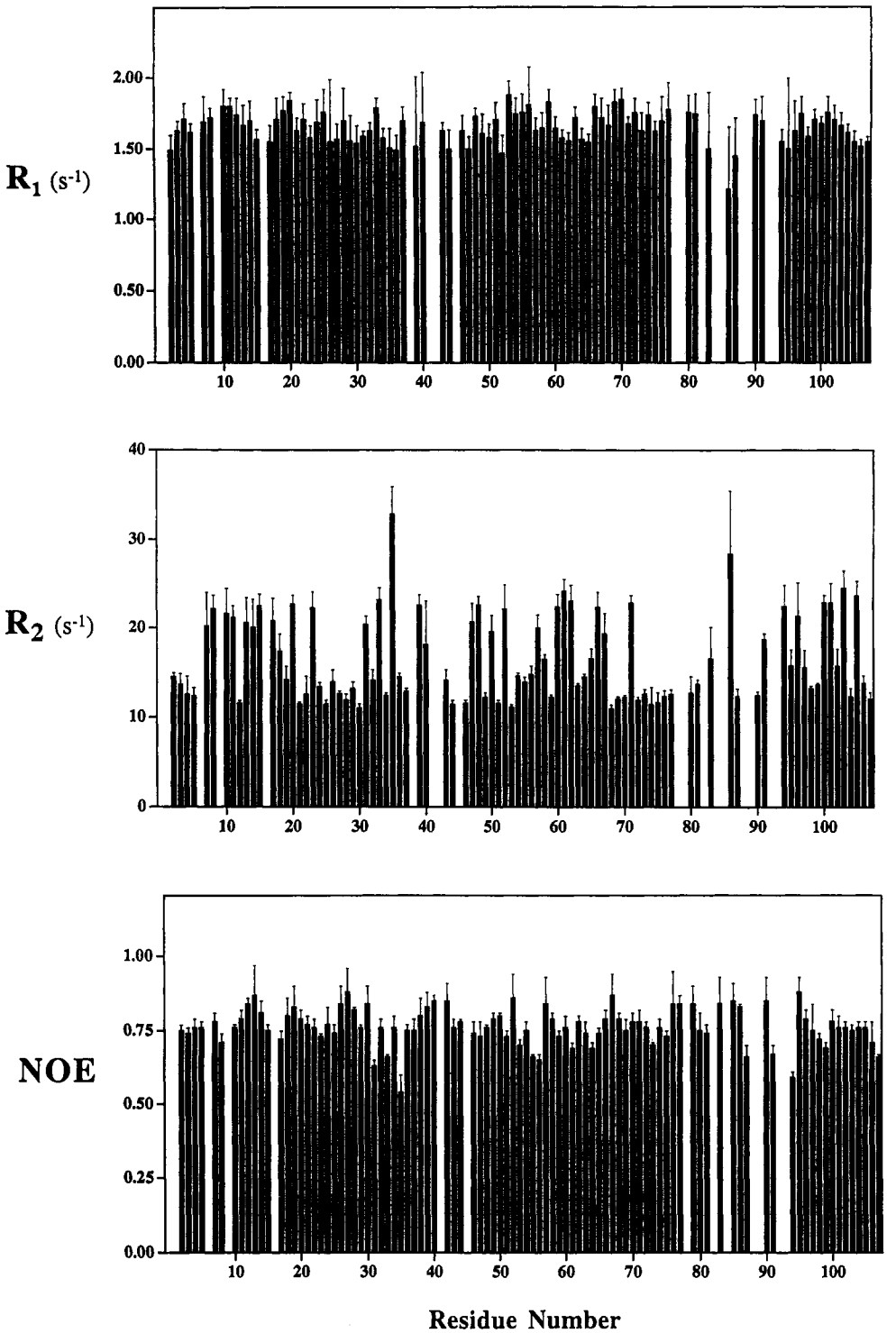

FIGURE 3: Plots of the measured ^{15}N relaxation parameters as a function of residue number: (a, top) spin–lattice relaxation rate constant (R_1); (b, middle) spin–spin relaxation rate constant (R_2); (c, bottom) heteronuclear NOE. Error bars represent standard deviations calculated from the covariance matrix of the optimized two- or three-parameter fit and validated by comparison to the Monte Carlo simulations (Palmer et al., 1991). Residues for which no results are shown correspond either to proline residues or to residues for which N–H cross-peaks could not be observed (see text).

vector. Whereas R_1, R_2, and NOE are all sensitive to internal motions on a time scale faster than the overall rotational correlation time, the R_2 values can also reflect internal motions occurring on a slower time scale, such as those arising due to chemical exchange or conformational averaging effects. These effects can cause line broadening and are quantified by the R_{ex} term in the model free formalism. It should be stressed that although R_2 is sensitive to motions on time scales slower than nanoseconds, these slower time scale motions are not experimentally accessible via the relaxation measurements used in this study. R_{ex} values arise during the course of optimization as a correction to R_2, the end result being a better overall fit for all experimental parameters. For this reason, care should be taken in quantitative evaluation of the R_{ex} values. To quantify processes occurring on the millisecond to microsecond time scale, other experiments, such as those that examine the field strength dependence of $T_{1\rho}$ (Deverell et al., 1970; Syzperski, 1992), are necessary. For an excellent discussion of relaxation measurements and the relevant time scales which may be accessed experimentally, the reader is

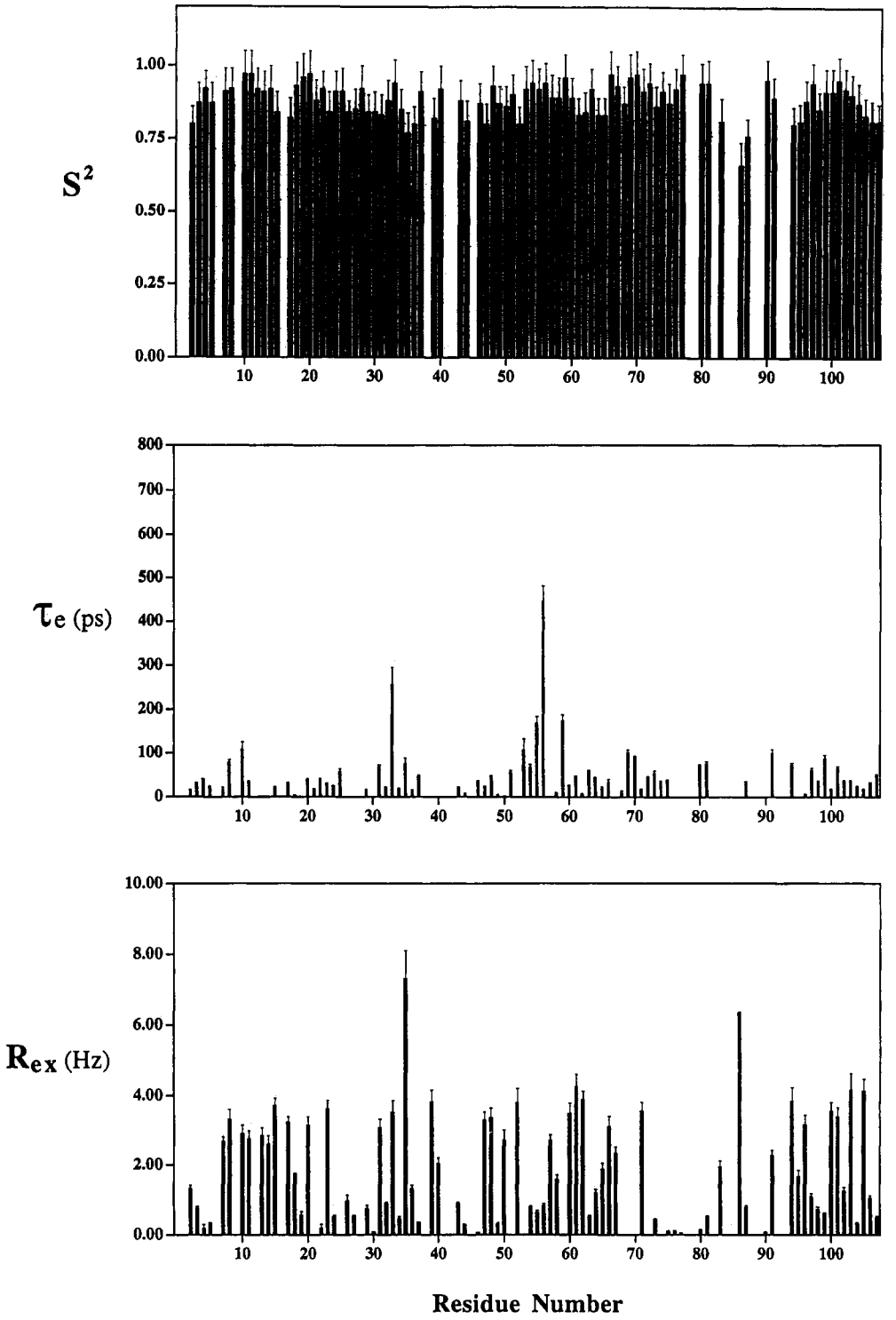

FIGURE 4: Plots of the optimized model free parameters a function of residue number: (a, top) generalized order parameter (S^2); (b, middle) effective correlation time for internal motions (τ_e); (c, bottom) chemical exchange line width (R_{ex}) in hertz. Standard deviations are estimated from the Monte Carlo simulations (Palmer et al., 1991).

referred to the work of Peng and Wagner (1992a). In the present study, we use R_{ex} values only for qualitative analysis of the FKBP-12 backbone dynamics.

Backbone Dynamics of FKBP-12. In the present study of FKBP-12, the R_1 and NOE values for most residues were found to fall within a narrow range (Figure 3), and the NOE values were close to the theoretical maximum of 0.82. These results suggest that the internal flexibility of the FKBP-12 backbone for the most part is limited on the nano- to picosecond time scale. Indeed, the optimized, generalized order parameters S^2 were found to be on average 0.88, indicating that the internal motions have small amplitudes. Order parameters are listed in Table I and shown graphically in Figures 4 and 5. Examination of the order parameters (S^2) for FKBP-12 indicates that there are no extended regions of high mobility within the protein. Upon close inspection, it is found that, for residues 2, 17, 35–36, 39, 44, 52, 83, 86–87, 94–95, and 106–107, the order parameters S^2 are slightly lower than the average value of 0.88 ± 0.06. These differences reflect slightly higher mobility in the N and C termini and the loop regions. However, the degree of mobility on the picosecond time scale observed at the N and C termini of FKBP-12 is relatively low compared

Table I: Optimized Model Free Parameters and Amide Proton Exchange Rates for FKBP-12

residue	S^2	τ_e (ps)	R_{ex} (Hz)	amide ^{1}H exchange[g]	residue	S^2	τ_e (ps)	R_{ex} (Hz)	amide ^{1}H exchange[g]
G1[a]				ND	V55[b]	0.92	168.89	0.63	–
V2[b]	0.80	16.51	1.32	–	I56[b]	0.94	446.40	0.82	–
Q3[b]	0.87	32.29	0.74	+	R57[d]	0.89		2.70	–
V4[b]	0.92	40.55	0.19	–	G58[b]	0.89	10.12	1.59	–
E5[b]	0.87	23.96	0.33	++	W59[e]	0.96	174.21		+
T6[a]				ND	E60[b]	0.89	26.89	3.48	+
I7[b]	0.91	15.49	2.68	+	E61[b]	0.83	47.68	4.25	+
S8[b]	0.92	79.04	3.31	+	G62[b]	0.84	7.74	3.88	+
P9[a]				ND	Y63[b]	0.92	58.42	0.51	++
G10[b]	0.97	107.53	2.90	–	A64[b]	0.83	44.42	1.20	+
D11[b]	0.97	36.11	2.75	–	Q65[b]	0.83	22.70	1.88	–
G12[c]	0.92			–	M66[b]	0.97	33.01	3.11	–
R13[d]	0.91		2.84	–	S67[d]	0.93		2.34	++
T14[d]	0.92		2.59	+	V68[e]	0.87	9.29		+
F15[b]	0.84	22.27	3.71	+	G69[e]	0.96	100.63		+
P16[a]				ND	Q70[e]	0.97	89.28		++
K17[b]	0.82	32.13	3.22	+	R71[b]	0.91	17.40	3.56	++
R18[b]	0.93	3.72	1.73	–	A72[e]	0.94	47.00		++
G19[d]	0.96		0.56	–	K73[b]	0.86	54.46	0.45	++
Q20[b]	0.97	40.78	3.15	+	L74[e]	0.91	36.85		++
T21[e]	0.88	17.36		+	T75[b]	0.87	39.14	0.11	++
C22[b]	0.92	40.55	0.19	++	I76[d]	0.92		0.12	++
V23[b]	0.84	30.79	3.61	++	S77[d]	0.97		0.05	++
V24[b]	0.91	24.78	0.51	++	P78[a]				ND
H25[e]	0.91	57.03		++	D79[f]				–
Y26[d]	0.84		0.95	–	Y80[b]	0.94	73.65	0.14	+
T27[d]	0.85		0.52	+	A81[b]	0.94	75.65	0.52	+
G28[c]	0.92			–	Y82[a]				–
M29[b]	0.84	16.43	0.74	+	G83[d]	0.81		1.95	–
L30[d]	0.84		0.08	–	A84[a]				ND
E31[b]	0.83	68.04	3.07	–	T85[f]				+
D32[b]	0.88	22.60	0.88	–	G86[d]	0.66		6.35	–
G33[b]	0.94	256.22	3.52	+	H87[b]	0.76	35.56	0.78	–
K34[b]	0.85	19.53	0.46	+	P88[a]				ND
K35[b]	0.77	75.95	7.30	–	G89[a]				–
F36[b]	0.80	16.51	1.32	+	I90[d]	0.95		0.08	+
D37[b]	0.91	45.90	0.35	–	I91[b]	0.89	99.34	2.28	+
S38[f]				–	P92[a]				ND
S39[d]	0.82		3.81	–	P93[a]				ND
R40[d]	0.92		2.03	–	H94[b]	0.80	72.51	3.84	–
D41[a]				ND	A95[d]	0.81		1.67	+
R42[f]				–	T96[b]	0.88	6.79	3.17	+
N43[b]	0.88	22.60	0.88	–	L97[b]	0.94	61.49	1.09	++
K44[b]	0.81	8.06	0.30	+	V98[b]	0.85	35.76	0.72	++
P45[a]				ND	F99[b]	0.91	87.90	0.60	++
F46[b]	0.87	35.74	0.06	+	D100[b]	0.91	17.40	3.56	++
K47[b]	0.80	23.65	3.29	+	V101[b]	0.95	65.00	3.39	++
F48[b]	0.93	47.84	3.35	+	E102[b]	0.92	36.41	1.25	++
M49[b]	0.87	5.10	0.30	–	L103[b]	0.90	36.51	4.16	+
L50[b]	0.86	1.70	2.71	+	L104[b]	0.87	23.96	0.33	++
G51[e]	0.90	56.89		–	K105[b]	0.83	17.99	4.13	++
K52[d]	0.80		3.79	+	L106[b]	0.81	30.92	1.05	++
Q53[e]	0.92	106.65		+	E107[b]	0.81	49.79	0.49	++
E54[b]	0.94	67.03	0.80	+					

[a] Not determined. [b] Data were optimized using the general form of the spectral density function (S^2, τ_e) and an additional term (R_{ex}) for line broadening. [c] Data were optimized using the simplified form of the spectral density function (S^2 only). [d] Data were optimized using the simplified form of the spectral density function and an additional term (R_{ex}) for line broadening. [e] Data were optimized using the general form of the spectral density function (S^2, τ_e). [f] Only heteronuclear NOEs could be obtained for residues S38, R42, D79, and T85. [g] ND = not determined; (–) = fast exchanging; (+) = slowly exchanging; (++) = slowest exchanging.

with that observed for other proteins (Kay et al., 1989; Clore et al., 1990a; Barbato et al., 1992; Kördel et al., 1992; Peng & Wagner, 1992a; Powers et al., 1992; Redfield et al., 1992; Schneider et al., 1992; Stone et al., 1992, 1993) and is consistent with our observations from NOE and amide exchange data (Table I) that the β-sheets of FKBP-12 extend to the protein termini.

It has recently been pointed out (Palmer et al., 1991) that calculation of τ_e may be in some instances unreliable. Bias in the value calculated for τ_e arises due to the dependence of τ_e on the uncertainty for the optimized value of S^2. Others (Stone et al., 1993) have found that for some residues τ_e values may adopt a wide range of values due to the insensitivity of the residual error to changes in τ_e. We have investigated this phenomenon with the present data and have found a similar insensitivity of the residual error to variations of τ_e. Although all values of τ_e reported here have met the required confidence criteria, for the reasons discussed above we have chosen not to attempt a quantitative interpretation of τ_e values. Qualitatively, significant values ($\tau_e > 50$ps) of τ_e are found in regions of regular secondary structure, as well as in regions which exhibit no regular secondary structure or are disordered. Thus, for FKBP-12 there appears to be no correlation between τ_e values and secondary structure.

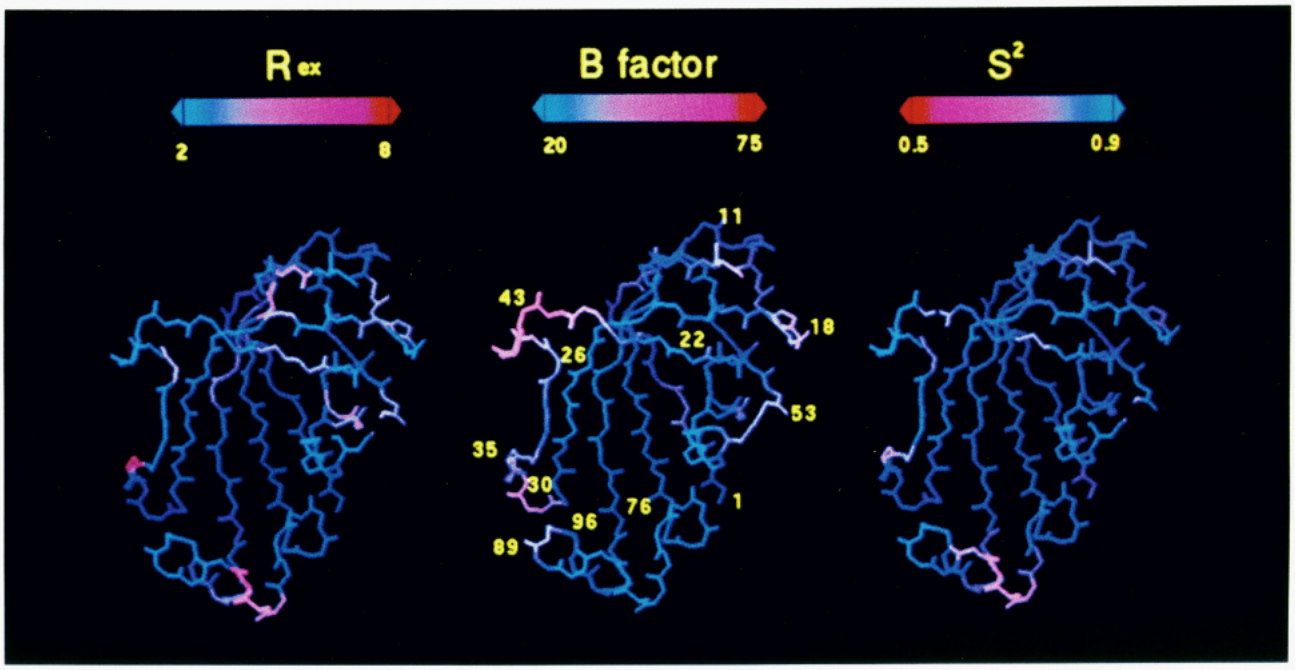

FIGURE 5: Backbone structures of FKBP-12 colored according to (left) R_{ex} value, (center) crystallographic B factors (M. M. Yamashita, S. H. Rotstein, M. A. Murcko, K. P. Wilson, J. Boger, J. A. Thomson, M. J. Fitzgibbon, and M. A. Navia, unpublished results), and (right) optimized order parameter S^2. The spectrum bars above each structure indicate color range and the values encompassed by each spectrum.

Although motions on the picosecond time scale appear relatively restricted throughout most of the FKBP-12 molecule, motions on the milli- to microsecond time scales, as indicated by larger exchange line widths (R_{ex}), are found in several regions of the protein. For many residues that are hydrogen-bonded and in well-defined β-sheets (such as residues 72–76), R_{ex} terms are found to be small (<2.0 Hz) (Table I and Figure 4). However, for some residues located in loops and at the C terminus (Figure 4), R_{ex} values are larger than 2 Hz, indicating internal motion on a milli- to microsecond time scale arising from conformational averaging and/or amide exchange effects. Low order parameters and high R_{ex} values are found for residue 35, which is located in a short segment of extended structure and may undergo conformational averaging, and for residue 86, which exhibits an attenuated amide resonance in H_2O spectra and may undergo very rapid amide exchange. Interestingly, some amides that are hydrogen-bonded in well-defined β-sheets exhibit high order parameters but have R_{ex} terms greater than 2.0 Hz. For example, in the β-strand from residues 97 to 103, residues 100–101 help form the core of the sheet, yet have R_{ex} terms above 3.0 Hz. This phenomenon has been observed previously (Redfield et al., 1992) and attributed to breathing motions of the β-sheet. However, as discussed above, the R_{ex} term alone provides no information regarding the precise time scale or amplitude of the motions.

Two NMR structures of uncomplexed FKBP-12 have been recently reported (Michnick et al., 1991; Moore et al., 1991). The solution structure of FKBP-12 complexed with the immunosuppressant ascomycin has also been determined by NMR methods to high resolution (Meadows et al., 1993). It was noted by Meadows et al. (1993) that the solution structures of the complexed and uncomplexed forms of FKBP-12 differed in certain regions. For example, in uncomplexed FKBP-12 (Moore et al. 1991; Lepre and Moore, unpublished results) residues 34–36 form a short segment of extended structure, followed by a disordered loop from residues 37 to 45. However, in the complex with ascomycin (Meadows et al., 1993) residues 36–39 are found to be in a short β-strand, followed by a loop from residues 40 to 45. Moreover, for residues 78–95 in the FKBP/ascomycin complex, a single turn of 3_{10} helix (residues 78–80) and two type II β-turns (residues 87–90 and 92–95) were found, whereas in uncomplexed FKBP-12, residues 78–95 were not well-defined due to a lack of NOE constraints. It was not known whether the differences in local structure observed for these regions were due to a simple lack of NOE data for the uncomplexed structure or, alternatively, due to stabilization of these regions as a consequence of protein–drug interactions in the complex structure.

In the present study, backbone mobility for several residues in both the 36–45 and 78–95 loops was found to be considerably higher than in other regions of uncomplexed FKBP-12. From an analysis of contacts between FKBP-12 and both ascomycin (Meadows et al., 1993) and FK506 (Van Duyne et al., 1993) it appears possible that interactions with the inhibitor play an important role in stabilizing elements of structure which are well-defined in the complex, yet ill-defined in the native protein. For example, the crystal structure reveals close contacts (<4.0 Å) between several regions of the FK506 molecule and residues 36 and 37 of FKBP-12. Also, hydrogen bonds exist between Asp37 O^{δ} and Phe36 $C^{\epsilon}H$ and between the C10 hydroxyl and C9 carbonyl groups of FK506, respectively. In the flap region (residues 78–95), many close contacts again exist between the protein and drug molecule [see Van Duyne et al. (1993)], and a hydrogen bond exists between Tyr82 OH and the C8 carbonyl of FK506. Since residues located in both regions (residues 34–45 and 78–95) are involved in ligand–protein interactions, it is likely that structural and dynamic changes occur in these regions upon ligand binding. Changes in the dynamic properties of these two loops may explain why more NOE constraints were observed in the FKBP-12–ascomycin complex and why this led to better defined local structure than found in uncomplexed FKBP-12. It should be interesting to compare the results of NMR relaxation studies in the free and bound forms of FKBP-12.

Comparison of Order Parameters with Temperature Factors. As first discussed by Clore et al. (1990a), comparison of relative order in solution versus crystal states is difficult,

due to the different manner in which order is quantified in the two environments. The generalized order parameter (S^2) and the correlation time for fast internal motions (τ_e) provide simple means to assess relative order and disorder within a molecule, without resorting to any particular model to describe the motion. In contrast, crystallographic *B* factors encompass several types of disorder, including both simple molecular vibrations and intrinsic lattice disorder. Unfortunately, it is not possible to distinguish between these two types of disorder with a single crystallographic measurement. In addition, *B* factors provide no indication of the relative time scales of molecular motion occurring in the crystal lattice, and crystal packing effects may also be responsible for order in regions of a protein which might possess much less order in solution. With these caveats in mind, it is interesting to compare the disorder present in solution with that observed in the crystal. Figure 5 shows the FKBP-12 backbone color-coded according to the *B* factors determined for bovine thymus FKBP (M. M. Yamashita, S. H. Rotstein, M. A. Murcko, K. P. Wilson, J. Boger, J. A. Thomson, M. J. Fitzgibbon, and M. A. Navia, unpublished results). The highest temperature factors are found for residues 41–45, with lesser, yet higher than average values found near residues 17–18, 31–34, 51–53, and 89–94. These results are in marked contrast to the results obtained from ^{15}N relaxation measurements, which indicate that motion on the picosecond time scale is greatest at residues 84–87 and that mobility in the loop from residues 41 to 45 is restricted. Examination of the crystal packing environment in the flap region (residues 78–95) indicates that close packing exists along residues 81–88 with an adjacent molecule in the lattice, whereas residues 89–92 are not influenced by crystal packing forces. It appears likely that any motion in the flap region from residues 81 to 88 is damped due to interactions with the neighboring protein molecule, causing this portion of the molecule to appear to possess a degree of order similar to that found for the rest of the protein. Thus, molecular motion described by the *B* factor in the crystal and order parameters characterizing disorder on the picosecond time scale in solution do not appear to correlate for the case of FKBP-12. This result is not surprising, given the different time scales over which these dynamic processes occur and the radically different environments in which the two measurements are made. In the few studies to date in which dynamics in solution have been compared to dynamics in the crystal, it has been shown that order parameters and *B* factors (RMS displacements) do correlate in some instances (Kördel et al., 1992) but in most cases show weak or no correlation (Clore et al., 1990a; Constantine et al., 1993; Stone et al., 1993). The present difficulty in correlating dynamics in the crystalline environment to dynamics in solution, for the reasons discussed above, underlines the importance of characterizing protein dynamics in solution. This is particularly true for the purposes of rational drug design, where an understanding of the molecular motions as well as the molecular structure of a drug target is critical to the design of potential therapeutic agents.

Conclusion. We have examined the backbone dynamics of FKBP-12 using ^{15}N relaxation measurements. Our results indicate that the internal flexibility of the well-defined β-sheet, including both the N and C termini, is restricted on the picosecond time scale. On the other hand, several residues in the 36–45 and 78–95 loops that surround the ligand binding sites exhibit higher mobility than those found in regions of regular secondary structure. These results are consistent with previous NMR structural studies of uncomplexed FKBP-12 (Michnick et al., 1991; Moore et al., 1991), in which the β-sheet appears well-defined but other regions which exhibit no regular secondary structure are poorly defined. Regions which exhibit the most variability in the solution structures also possess the lowest order parameters and highest R_{ex} terms. It appears likely that differences in structure and backbone dynamics between free and FK506-bound FKBP-12 arise due to stabilizing interactions when the ligand binds to protein. Comparison of this work with backbone ^{15}N relaxation studies of the FKBP-12 FK506 complex should provide more insight into the structural and dynamic consequences of FK506 binding to FKBP. Such work is in progress.

ACKNOWLEDGMENT

We thank Dr. Johan Kördel, Dr. Arthur G. Palmer, Dr. Mark Rance, and Dr. Gerhard Wagner for helpful discussions. We also thank Dr. Manuel Navia and Sergio Rotstein for access to X-ray crystallographic data prior to publication, Dr. Arthur G. Palmer and Dr. David Pearlman for providing us with software routines, and Dr. Mark Murcko and Jim Griffith for computational assistance. We also thank Matthew Fitzgibbon for assistance in the protein purification.

REFERENCES

Appelt, K., Bacquet, R. J., Bartlett, C. A., Booth, C. L. J., Freer, S. T., Fuhry, M. A. M., Gehring, M. R., Herrmann, S. M., Howland, E. F., Janson, C. A., Jones, T. R., Kan, C.-C., Kathardekar, V., Lewis, K. K., Marzoni, G. P., Matthews, D. A., Mohr, C., Moomaw, E. W., Morse, C. A., Oatley, S. J., Ogden, R. C., Reddy, M. R., Reich, S. H., Schoettlin, W. S., Smith, W. W., Varney, M. D., Villafranca, J. E., Ward, R. W., Webber, S., Webber, S. E., Welsh, K. M., & White, J. (1991) *J. Med. Chem. 34*, 1925–1934.

Baldwin, J. J., Ponticello, G. S., Anderson, P. S., Christy, M. E., Murcko, M. A., Randall, W. C., Schwam, H., Sugrue, M. F., Springer, J. P., Gautheron, P., Grove, J., Mallorga, P., Viader, M.-P., McKeever, B. M., & Navia, M. A. (1989) *J. Med. Chem. 32*, 2510–2513.

Barbato, G., Ikura, M., Kay, L. E., Pastor, R. W., & Bax, A. (1992) *Biochemistry 31*, 5269–5278.

Bax, A., Ikura, M., Kay, L. E., Torchia, D. A., & Tschudin, R. (1990) *J. Magn. Reson. 86*, 304–318.

Berglund, H., Kovács, H., Dahlman-Wright, K., Gustafsson, J., & Härd, T. (1992) *Biochemistry 31*, 12001–12011.

Bierer, B. E., Somers, P. K., Wandless, T. J., Burakoff, S. J., & Schreiber, S. L. (1990) *Science 250*, 556–559.

Braunschweiler, L., Bodenhausen, G., & Ernst, R. R. (1983) *Mol. Phys. 48*, 535–560.

Clore, G. M., Driscoll, P. C., Wingfield, P. T., & Gronenborn, A. M. (1990a) *Biochemistry 29*, 7387–7401.

Clore, G. M., Szabo, A., Bax, A., Kay, L. E., Driscoll, P. C., & Gronenborn, A. M. (1990b) *J. Am. Chem. Soc. 112*, 4989–4991.

Constantine, L. L., Friedrichs, M. S., Goldfarb, V., Jeffrey, P. D., Sheriff, S., & Mueller, L. (1993) *Proteins 15*, 290–311.

Deverell, C., Morgan, R. E., & Strange, J. H. (1970) *Mol. Phys. 18*, 553–559.

Fesik, S. W., Gampe, R. T., Eaton, H. L., Gemmecker, G., Olejniczak, E. T., Neri, P., Holzman, T. F., Egan, D. A., Edalji, R., Simmer, R., Helfrich, R., Hochlowski, J., & Jackson, M. (1991) *Biochemistry 30*, 6574–6583.

Fesik, S. W., Neri, P., Meadows, R., Olejniczak, E. T., & Gemmecker, G. (1992) *J. Am. Chem. Soc. 114*, 3165–3166.

Fischer, G., Wittmann-Liebold, B., Lang, K., Kiefhaber, T., & Schmid, F. X. (1989) *Nature 337*, 476–478.

Flanagan, W. M., Corthesy, B., Bram, R. J., & Crabtree, G. R. (1991) *Nature 352*, 803–807.

Griesinger, C., Otting, G., Wüthrich, K., & Ernst, R. R. (1988) *J. Am. Chem. Soc. 110*, 7870–7872.

Hiyama, Y., Niu, C.-H., Silverton, J. V., Bavoso, A., & Torchia, D. A. (1988) *J. Am. Chem. Soc. 110*, 2378–2383.
Hsu, V. L., & Armitage, I. M. (1992) *Biochemistry 31*, 12778–12784.
Kallen, J., & Walkinshaw, M. D. (1992) *FEBS Lett. 300*, 286–290.
Kallen, J., Spitzfaden, C., Zurini, M. G. M., Wider, G., Widmer, H., Wüthrich, K., & Walkinshaw, M. D. (1991) *Nature 353*, 276–279.
Kay, L. E., Torchia, D. A., & Bax, A. (1989) *Biochemistry 28*, 8972–8979.
Ke, H., Zydowsky, L. D., Liu, J., & Walsh, C. T. (1991) *Proc. Natl. Acad. Sci. U.S.A. 88*, 9483–9487.
Kördel, J., Skelton, N. J., Akke, M., Palmer, A. G., & Chazin, W. J. (1992) *Biochemistry 31*, 4856–4866.
Kuntz, I. D. (1992) *Science 257*, 1078–1082.
Lepre, C. A., Thomson, J. A., & Moore, J. M. (1992) *FEBS Lett. 302*, 89–96.
Lipari, G., & Szabo, A. (1982a) *J. Am. Chem. Soc. 104*, 4546–4559.
Lipari, G., & Szabo, A. (1982b) *J. Am. Chem. Soc. 104*, 4559–4570.
Liu, J., Farmer, J. D. J., Lane, W. S., Friedman, J., Weissman, I., & Schreiber, S. L. (1991) *Cell 66*, 807–815.
Liu, J., Albers, M. W., Wandless, T. J., Luan, S., Alberg, D. G., Belshaw, P. J., Cohen, P., MacKintosh, C., Klee, C. B., & Schreiber, S. L. (1992) *Biochemistry 31*, 3896–3901.
Maniatis, T., Fritsch, E. F., & Sambrook, J. (1986) *Molecular Cloning: A Laboratory Manual*, Cold Spring Harbor Laboratory, Cold Spring Harbor, NY.
Marion, D., & Wüthrich, K. (1983) *Biochem. Biophys. Res. Commun. 113*, 967–974.
Meadows, R. P., Nettesheim, D. G., Xu, R. X., Olejniczak, E. T., Petros, A. M., Holzman, T. F., Severin, J., Gubbins, E., Smith, H., & Fesik, S. W. (1993) *Biochemistry 32*, 754–765.
Meiboom, S., & Gill, D. (1958) *Rev. Sci. Instrum. 29*, 688–691.
Messerle, B. A., Wider, G., Otting, G., Weber, C., & Wüthrich, K. (1989) *J. Magn. Reson. 85*, 608–613.
Michnick, S. W., Rosen, M. K., Wandless, T. J., Karplus, M., & Schreiber, S. L. (1991) *Science 252*, 836.
Moore, J. M., Peattie, D. A., Fitzgibbon, M. J., & Thomson, J. A. (1991) *Nature 351*, 248–250.
Navia, M. A., & Murcko, M. A. (1992) *Curr. Opin. Struct. Biol. 2*, 202–210.
Norwood, T. J., Boyd, J., Heritage, J. E., Soffe, N., & Campbell, I. (1990) *J. Magn. Reson. 87*, 488–501.
Palmer, A. G., Rance, M., & Wright, P. E. (1991) *J. Am. Chem. Soc. 113*, 4371–4380.
Peng, J. W., & Wagner, G. (1992a) *Biochemistry 31*, 8571–8586.
Peng, J. W., & Wagner, G. (1992b) *J. Magn. Reson. 98*, 308–332.
Petros, A. M., Gemmecker, G., Neri, P., Olejniczak, E. T., Nettesheim, D., Xu, R. X., Gubbins, E. G., Smith, H., & Fesik, S. W. (1992a) *J. Med. Chem. 35*, 2467–2473.
Petros, A. M., Kawai, M., Luly, J. R., & Fesik, S. W. (1992b) *FEBS Lett. 308*, 309–314.
Pflügl, G., Kallen, J., Schirmer, T., Jansonius, J. N., Zurini, M. G. M., & Walkinshaw, M. D. (1993) *Nature 361*, 91.
Powers, R., Clore, G. M., Stahl, S. J., Wingfield, P. T., & Gronenborn, A. (1992) *Biochemistry 31*, 9150–9157.
Rance, M., & Wright, P. E. (1986) *J. Magn. Reson. 66*, 372–378.
Redfield, C., Boyd, J., Smith, L. J., Smith, R. A. G., & Dobson, C. M. (1992) *Biochemistry 31*, 10431–10437.
Rosen, M. K., & Schrieber, S. L. (1992) *Angew. Chem., Int. Ed. Engl. 31*, 384–400.
Rosen, M. K., Michnick, S. W., Karplus, M., & Schreiber, S. L. (1991) *Biochemistry 30*, 4774–4789.
Schneider, D. M., Dellwo, M. J., & Wand, A. J. (1992) *Biochemistry 31*, 3645–3652.
Schreiber, S. L. (1991) *Science 251*, 283–287.
Shaka, A. J., & Keeler, J. (1987) *Prog. NMR Spectrosc. 19*, 44–129.
Sigal, N. H., & Dumont, F. J. (1992) *Annu. Rev. Immunol. 10*, 519–560.
Skelton, N. J., Kördel, J., Akke, M., & Chazin, W. J. (1992) *J. Mol. Biol. 227*, 1100–1117.
Spitzfaden, C., Weber, H.-P., Braun, W., Kallen, J., Wider, G., Widmer, H., Walkinshaw, M. D., & Wüthrich, K. (1992) *FEBS Lett. 300*, 291–300.
Stone, M. J., Fairbrother, W. J., Palmer, A. G., Reizer, J., Saier, M. H. J., & Wright, P. E. (1992) *Biochemistry 31*, 4394–4406.
Stone, M. J., Chandrasekhar, K., Holmgren, A., Wright, P. E., & Dyson, H. J. (1993) *Biochemistry 32*, 426–435.
Studier, F. W., & Moffat, B. A. (1986) *J. Mol. Biol. 189*, 113–130.
Studier, F. W., Rosenberg, A. H., Dunn, J. J., & Dubendorff, J. W. (1990) *Methods Enzymol. 185*, 60–89.
Szyperski, T. (1992) Ph.D. Thesis, ETH Zurich.
Thériault, Y., Logan, T. M., Meadows, R., Yu, L., Olejniczak, E. T., Holzman, T. F., Simmer, R. L., & Fesik, S. W. (1993) *Nature 361*, 88.
Van Duyne, G. D., Standaert, R. F., Karplus, P. A., Schreiber, S. L., & Clardy, J. (1991a) *Science 252*, 839.
Van Duyne, G. D., Standaert, R. F., Schreiber, S. L., & Clardy, J. (1991b) *J. Am. Chem. Soc. 113*, 7433–7434.
Van Duyne, G. D., Standaert, R. F., Karplus, P. A., Schreiber, S. L., & Clardy, J. (1993) *J. Mol. Biol. 229*, 105–124.
Venters, R. A., Calderone, T. L., Spicer, L. D., & Fierke, C. A. (1991) *Biochemistry 30*, 4491–4494.
Weber, C., Wider, G., von Freyberg, B., Traber, R., Braun, W., Widmer, H., & Wüthrich, K. (1991) *Biochemistry 30*, 6563–6574.
Wüthrich, K., Spitzfaden, C., Memmert, K., Widmer, H., & Wider, G. (1991) *FEBS Lett. 285*, 237–247.